

## Populations of $B^2\Sigma_u^+$ and $X^2\Sigma_g^+$ electronic states of molecular nitrogen ions in air determined by fluorescence measurement

Quanjun Wang<sup>1</sup>, Rao Chen<sup>1</sup>, Yuxuan Zhang<sup>1</sup>, Xiaozhen Wang<sup>2</sup>, Chunlin Sun<sup>2</sup>, Pengji Ding<sup>1</sup>, Zuoye Liu<sup>1,\*</sup> and Bitao Hu<sup>1,†</sup>

<sup>1</sup>*School of Nuclear Science and Technology, Lanzhou University, Lanzhou 73000, People's Republic of China*

<sup>2</sup>*College of Chemistry and Chemical Engineering, Lanzhou University, Lanzhou 73000, People's Republic of China*



(Received 23 May 2020; revised 1 March 2021; accepted 10 March 2021; published 24 March 2021)

We carry out a combined experimental and numerical investigation on the population distribution between the ground state and the excited state of molecular nitrogen ions in an 800-nm laser field. Efficient population transfers between the ground state  $N_2^+(X^2\Sigma_g^+, \nu = 0)$  and the excited state  $N_2^+(B^2\Sigma_u^+, \nu' = 0)$  occur with a 400-nm time-delayed pulse, resulting in an enhanced fluorescence at 391 and 428 nm. The population distribution between the ground state  $N_2^+(X^2\Sigma_g^+, \nu = 0)$  and the excited state  $N_2^+(B^2\Sigma_u^+, \nu' = 0)$  is extracted from the fluorescence enhancement factor. The results show that the population of  $N_2^+(X^2\Sigma_g^+, \nu = 0)$  decreases when the laser exceeds 2.1 mJ in our experiment. Our study provides a method to check the population information of both excited and ground states experimentally in a strong-field-induced plasma of ionized nitrogen molecules.

DOI: [10.1103/PhysRevA.103.033117](https://doi.org/10.1103/PhysRevA.103.033117)

### I. INTRODUCTION

Intense femtosecond laser pulses launched in air experience filamentary propagation, forming a bright channel of underdense plasma [1,2]. The typical laser intensity inside the plasma is around  $10^{13}$ – $10^{14}$  W/cm<sup>2</sup> for an 800-nm laser pulse with different focus conditions [3–5]. Multiphoton and/or tunnel ionization are fundamental processes under such a laser field. The ionization rate is highly sensitive to the ionization potentials and orbital geometries of molecules for both multiphoton and tunnel ionization, providing new methods of imaging molecular orbitals [6–9]. Due to the multielectron effects and the close ionization potentials between the outermost and a few lower-lying orbitals, inner-valence electrons could be ionized in strong laser fields [10–12]. A direct consequence of the multiorbital ionization is that not only ground-state but also excited molecular ions exist in the plasma. A basic example is the nitrogen molecule, whose electronic ground-state configuration is  $KK(\sigma_g 2s)^2(\sigma_u 2s)^2(\pi_u 2p)^2(\sigma_g 2p)^2$ . The emission of an electron from  $(\pi_u 2p)$  and  $(\sigma_u 2s)$  orbitals leaves the ions in the excited ( $A^2\Pi_u$ ) and ( $B^2\Sigma_u^+$ ) states, respectively, which differ in energy by less than 4 eV from the ionic ground state ( $X^2\Sigma_g^+$ ) [12].

Because molecular ions in the excited states can decay to the ground state by spontaneous fluorescence emissions, discrete fluorescence lines have been used as a tool to identify the excited electronic states, and the emission intensity can be employed to estimate the number of excited ions [13,14]. However, the population information of the ground state is hard to determine by a simple fluorescence measurement. As a commonly accepted assumption, the ionization probabilities of each ionic state are exponentially suppressed by their corre-

sponding ionization potentials [15–18]. The populations in the excited states are much less than those in the ground state. But recent observations of “lasing” at 391 nm from  $N_2^+(B^2\Sigma_u^+)$  to  $N_2^+(X^2\Sigma_g^+)$  in air or pure nitrogen gas seem to challenge this assumption [5,19–22]. It is necessary to explore the population distribution between the ground and excited states, which is central to the interpretation of the “lasing” action above. A detailed understanding is also important for the fundamental excitation and ionization processes induced by strong laser fields.

In this article, we developed a pump-probe method to detect the population of both the ground vibrational state  $N_2^+(X^2\Sigma_g^+, \nu = 0)$  and excited state  $N_2^+(B^2\Sigma_u^+, \nu' = 0)$  in air plasma. After photoionization, the nitrogen molecular ions in the ground state are efficiently transferred to the excited state through the one-photon, near-resonant process with a weak 400-nm pulse, leading to enhanced fluorescence emissions at 391 and 428 nm. The population information of the ground state  $N_2^+(X^2\Sigma_g^+, \nu = 0)$  is involved in the transfer process and can be extracted.

### II. EXPERIMENTAL SETUP

The experiment was carried out using a pump-probe scheme similar to the one described in Ref. [23]. A linearly polarized 800-nm laser provided by a commercial Ti:sapphire laser system (Legend Elite-Duo, Coherent Inc.) had a maximal energy of 5.8 mJ at a 1 kHz repetition rate. The spectrum had a 11-nm spectral width full width at half maximum (FWHM), and a transform-limited pulse duration  $\tau_e$  of 85 fs. The laser beam was split into two arms (1:1) by a beam splitter. One beam serving as the pump pulse could excite and ionize the nitrogen molecules in air. The pump energy was tuned by a continuously variable neutral density attenuator. The other beam was frequency doubled by a 200- $\mu$ m-thick beta barium borate ( $\beta$ -BBO) crystal to generate a 400-nm

\*zyl@lzu.edu.cn

†hubt@lzu.edu.cn

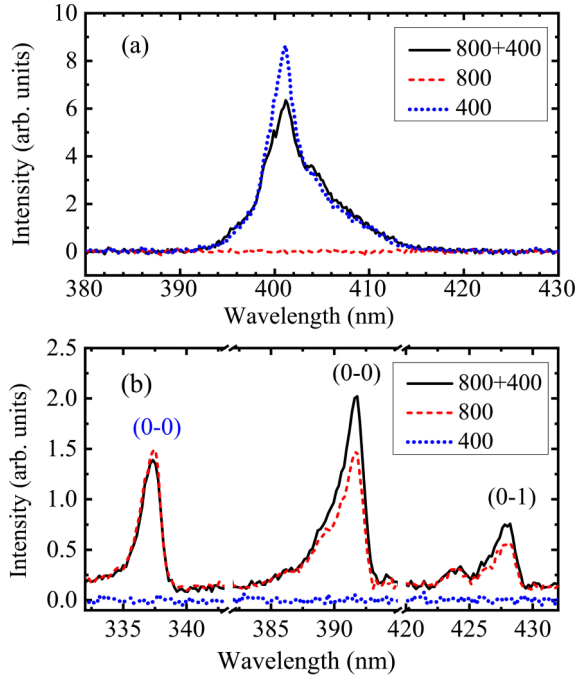


FIG. 1. (a) The forward emission and (b) typical fluorescence spectra, measured under both 800- and 400-nm pulses (black solid line), only the 800-nm pulse (red dashed line), and the 400-nm pulse (blue dotted line). The energy of the 800-nm pump pulse is 2.7 mJ and the time delay is 1 ps.

pulse. The energy of the 400-nm pulse after the two dichroic mirrors was measured to be 102  $\mu$ J. The FWHM of the 400-nm pulse was 3.5 nm. Assuming a transform-limited Gaussian pulse distribution, we obtained a minimum pulse duration  $\tau_f$  of 67 fs. The two pulses were combined by another dichroic mirror and then were collinearly focused by a fused silica lens with a focal length of 150 mm. The time delay between the pump and probe pulses was varied with a motorized optical delay line. After the interaction, the two pulses were reflected by several dichroic mirrors and focused again. In this way, we checked the forward emission. The plasma fluorescence was collected by a spherical mirror ( $f = 100$  mm), which was set on a three-dimensional moving stage to obtain the maximum signal. A fiber was used to couple the signal (forward emission or fluorescence) into a fiber-pigtailed spectrometer (ocean optics, USB 4000+) with a spectral resolution of 0.25 nm.

### III. RESULTS AND DISCUSSIONS

Figure 1(a) shows the spectra measured in the forward direction. The 800-nm pulse with 2.7 mJ energy generates a bright plasma in air. Because the pump pulse is not strong enough, no supercontinuum is detected in the region of 360–450 nm, and no “lasing” action is observed at 391 or 428 nm. Then the 400-nm pulse passes through the air plasma on a time delay of 1 ps to avoid ionization enhancement induced by the overlap of these two pulses [24]. The 400-nm pulse with a bandwidth (FWHM) of 3.5 nm does not cover the wavelength of 391 nm, and there is no amplification of the 400-nm pulse. The spectral intensity of the 400-nm pulse in the pres-

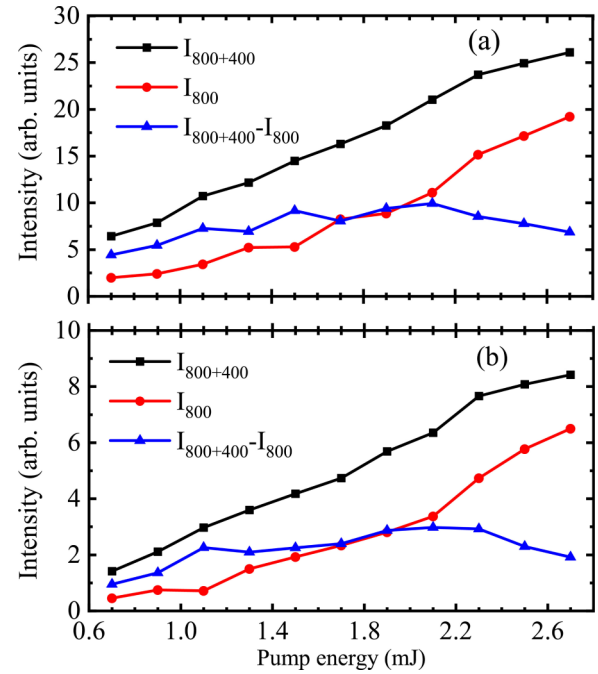


FIG. 2.  $I_{800+400}$  (black square),  $I_{800}$  (red circle), and  $I_{800+400} - I_{800}$  (blue upper triangle) of (a) 391 nm and (b) 428 nm as a function of 800-nm pump energy.

ence of the pump pulse (black solid line) is weaker than its original spectrum (blue dotted line), which is attributed to the defocusing effect of the low-density plasma [25]. The fluorescence signals are too weak to detect in the forward direction. We obtain the typical fluorescence spectra (red dashed line) on the side of the plasma with an accumulation of a thousand laser shots, as shown in Fig. 1(b). The discrete lines at 391 and 428 nm are clearly displayed, which correspond, respectively, to transitions (0-0) and (0-1) between the vibrational levels of the excited state  $N_2^+(B^2\Sigma_u^+)$  and ground state  $N_2^+(X^2\Sigma_g^+)$  [13]. The fluorescence is hardly detected with a 400-nm pulse alone, indicating that a weak 400-nm pulse could not efficiently ionize nitrogen molecules. Meanwhile, the emissions at 391 and 428 nm are enhanced with the existence of a weak 400-nm pulse (black solid line) in Fig. 1(b).

The fluorescence signals of 391 and 428 nm varying with pump energy were investigated on a time delay of 1 ps, as shown in Figs. 2(a) and 2(b). The signal intensities induced by the 800- and 400-nm pulses are labeled as  $I_{800+400}$ , and those induced only by the 800-nm pump pulse are labeled as  $I_{800}$ .  $I_{800+400}$  and  $I_{800}$  of 391 nm both rise with the pump energy from 0.7 to 2.7 mJ. Interestingly, the difference of  $I_{800+400} - I_{800}$  first increases and then decreases, leaving a maximum value around 2.1 mJ. Similar results can be found for the 428-nm line in Fig. 2(b). As commonly accepted, the fluorescence signal of the first negative band in a molecular nitrogen ion is proportional to the total number of ions in the excited state [13,14,26–28]. Arévalo and Becker estimated the number of excited-state ions  $N_2^+(B^2\Sigma_u^+, v' = 0)$  by numerical simulations of the filament formation of a Ti:sapphire femtosecond laser pulse in nitrogen molecular gas. The flu-

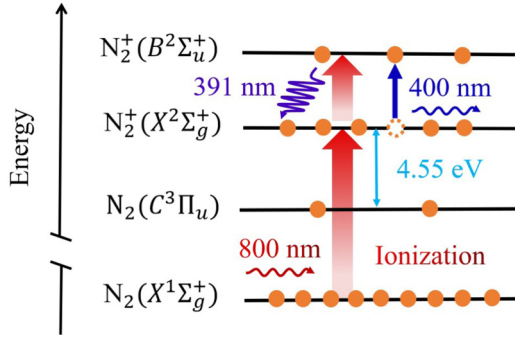


FIG. 3. Energy levels of  $N_2$  and  $N_2^+$ , and the near-resonant interaction of a 400-nm pulse and  $B^2\Sigma_u^+ - X^2\Sigma_g^+$  two-level system.

orescence signal in their calculation is approximately equal to the number of excited-state ions; the numerical results agreed well with the experimental data of a 391-nm fluorescence signal at two values of pressure, 400 and 760 Torr, with the laser energy ranging from 1 to 30 mJ and 1 to 9 mJ, respectively [14]. In our case, we have  $I_{800}^{391} + I_{800}^{428} \simeq N_B^i$ , where  $N_B^i$  is the population of  $N_2^+(B^2\Sigma_u^+, \nu' = 0)$  generated by the 800-nm pump pulse alone, i.e., initial population (density). Similarly, there are  $I_{800+400}^{391} + I_{800+400}^{428} \simeq N_B^f$ , where  $N_B^f$  denotes the population of  $N_2^+(B^2\Sigma_u^+, \nu' = 0)$  induced by both the 800- and 400-nm laser pulse, i.e., final population (density).

As illustrated in Fig. 3, the nitrogen molecules are populated to the  $B^2\Sigma_u^+$  and  $X^2\Sigma_g^+$  states of  $N_2^+$  by tunnel ionization under an 800-nm laser field. The 400-nm pulse causes strong couplings between the  $X^2\Sigma_g^+(\nu = 0)$  and  $B^2\Sigma_u^+(\nu' = 0)$  states of  $N_2^+$ , which result in a population redistribution of these two states. Besides, the 400-nm pulse could ionize excited nitrogen molecules, increasing the number of molecular ions. The emission intensity of 337 nm, originating from the excited molecular level  $N_2(C^3\Pi_u)$ , has a reduction in Fig. 1(b) compared to that with an 800-nm pulse alone. This phenomenon has been investigated and used to measure the formation time of the excited neutral nitrogen molecules [24]. On a time delay of 1 ps, the intensity reduction is quite slight, and much smaller than the enhancement of emission of 391 or 428 nm. The increased number of ions from the excited neutral nitrogen molecules is ignored and the population of  $N_2^+(X^2\Sigma_g^+, \nu = 0)$  and  $N_2^+(B^2\Sigma_u^+, \nu' = 0)$  is considered to be unchanged after an interaction with the 400-nm pulse. We get

$$N_X^i + N_B^i = N_X^f + N_B^f, \quad (1)$$

where  $N_X^i$  and  $N_X^f$  are the initial and final population of  $N_2^+(X^2\Sigma_g^+, \nu = 0)$ , respectively.

After efficient couplings,  $\lambda N_X^i$  are transferred to  $N_2^+(B^2\Sigma_u^+, \nu' = 0)$ .  $\lambda$  is defined as

$$\lambda = \frac{N_B^f - N_B^i}{N_X^i}. \quad (2)$$

Based on Eq. (1),  $\lambda$  can be expressed as

$$\lambda = \frac{n_B^f - n_B^i}{n_X^i}, \quad (3)$$

where  $n_B^f$ ,  $n_B^i$ , and  $n_X^i$  are the final and initial relative population of  $N_2^+(B^2\Sigma_u^+, \nu' = 0)$ , and the initial relative population of  $N_2^+(X^2\Sigma_g^+, \nu = 0)$ , respectively.  $n_B^f = \frac{N_B^f}{N_X^i + N_B^f}$ , for example. A fluorescence enhancement factor  $\eta$  is written as

$$\eta = \frac{I_{800+400}^{391} + I_{800+400}^{428}}{I_{800}^{391} + I_{800}^{428}} - 1 = \frac{n_B^f}{n_B^i} - 1. \quad (4)$$

Using Eq. (3), we obtain

$$\eta = \frac{\lambda n_X^i}{n_B^i}. \quad (5)$$

The relative populations satisfy

$$n_B^i - n_X^i = w_1, \quad (6a)$$

$$n_B^i + n_X^i = 1, \quad (6b)$$

and

$$n_B^f - n_X^f = w_2, \quad (7a)$$

$$n_B^f + n_X^f = 1, \quad (7b)$$

with  $w_1$  and  $w_2$  respectively being the initial and final relative population difference. The relative population  $\lambda$  and  $\eta$  can be rewritten by  $w_1$  and  $w_2$ . Here, the enhanced factor reads

$$\eta = \frac{w_2 - w_1}{1 + w_1}. \quad (8)$$

Next, we investigate the relationship of  $w_1$  and  $w_2$  by solving two-level optical Bloch equations. The states  $N_2^+(X^2\Sigma_g^+, \nu = 0)$  and  $N_2^+(B^2\Sigma_u^+, \nu' = 0)$  constitute a two-level system in the air plasma. Interactions between the two-level system and the 400-nm laser pulse are described by the optical Bloch equations under the slowly varying amplitude approximation and rotating-wave approximation [29,30],

$$\frac{\partial u}{\partial t} = -\Delta v - \Gamma u, \quad (9a)$$

$$\frac{\partial v}{\partial t} = \Delta u + \Omega w - \Gamma v, \quad (9b)$$

$$\frac{\partial w}{\partial t} = -\Omega v - \Gamma(1 + w), \quad (9c)$$

where  $u$  and  $v$  denote dispersion and absorption terms;  $w$  is the relative population difference between the upper and lower energy level.  $\Delta = \omega_{BX} - \omega$ , with  $\omega_{BX}$  and  $\omega$  being the angular frequency of the transition from  $N_2^+(B^2\Sigma_u^+, \nu' = 0)$  to  $N_2^+(X^2\Sigma_g^+, \nu = 0)$  and the angular frequency of a 400-nm pulse, respectively.  $\Gamma = \frac{1}{\tau_r}$ , and  $\tau_r = 58 \times 10^{-9}$  s is the radiative lifetime [31]. Recently, a fast decay process with  $\tau_r = 6 \times 10^{-10}$  s has been observed [26]. Without loss of generality,  $\Gamma$  is taken as a parameter and set to be  $10^{10} \text{ s}^{-1}$ .  $\Omega(t) = \frac{\mu}{\hbar} E_0 f(t)$  is the Rabi frequency, where  $\mu$  denotes the electronic transition moment with a value of 1.7 D [32].  $E_0$

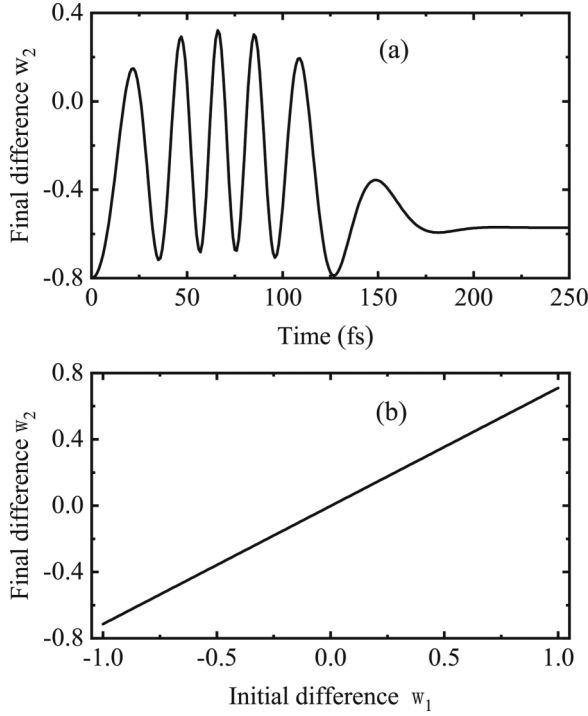


FIG. 4. (a) The temporal evolution of the relative population difference  $w_2$  under the 400-nm laser field with an intensity of  $4.7 \times 10^{12}$  W/cm<sup>2</sup>. (b) The final  $w_2$  as a function of  $w_1$ .

and  $f(t)$  are the peak and the envelope of the 400-nm laser pulse, respectively. The electric field takes the form

$$E(t) = E_0 f(t) \cos \omega t, \quad (10)$$

$$f(t) = e^{-2 \ln 2 \left(\frac{t}{\tau_f}\right)^2}. \quad (11)$$

Here,  $E_0 = \sqrt{\frac{2I_p}{c\epsilon_0}}$ , where  $I_p$ ,  $\epsilon_0$ ,  $c$ , and  $\tau_f$  are the laser peak intensity, the vacuum permittivity, light speed, and laser pulse duration, respectively. The 400-nm laser peak intensity (i.e.,  $4.7 \times 10^{12}$  W/cm<sup>2</sup>) and duration (i.e., 67 fs) are taken to be the same as the experimental parameter.

First, we assume that 10% of the molecular nitrogen ions populate in the  $N_2^+(B^2\Sigma_u^+, \nu' = 0)$  and 90% populate in the  $N_2^+(X^2\Sigma_g^+, \nu = 0)$  state; the initial relative population difference  $w_1$  is  $-0.8$ . Both  $u_1$  and  $v_1$  are 0 as there is no coupling between  $N_2^+(B^2\Sigma_u^+)$  and  $N_2^+(X^2\Sigma_g^+)$  in the 800-nm laser field. The optical Bloch equations (9a)–(9c) are solved numerically. In our calculation, the interaction between the 400-nm pulse and two-level system begins at  $-\tau_f$ , which corresponds to time zero in Fig. 4(a). It is seen that the final relative population difference is larger than  $-0.8$ , which means that the population in the  $N_2^+(X^2\Sigma_g^+, \nu = 0)$  state is transferred to  $N_2^+(B^2\Sigma_u^+, \nu' = 0)$ , leading to enhanced fluorescence emissions at 391 and 428 nm. The relative population difference oscillates before it finally converges to a value close to  $-0.6$ . Near the peak of the 400-nm laser, the population difference oscillates with a period of 20 fs. As is well known, the oscillation period is  $T = \frac{2\pi}{\sqrt{\Omega^2 + \Delta^2}}$  for a rectangular pulse [29]. If we regard the 400-nm electric field close to the peak as a constant, by using  $\Omega = \frac{\mu}{\hbar} E_0$  the calculated  $T$  is 19 fs. This

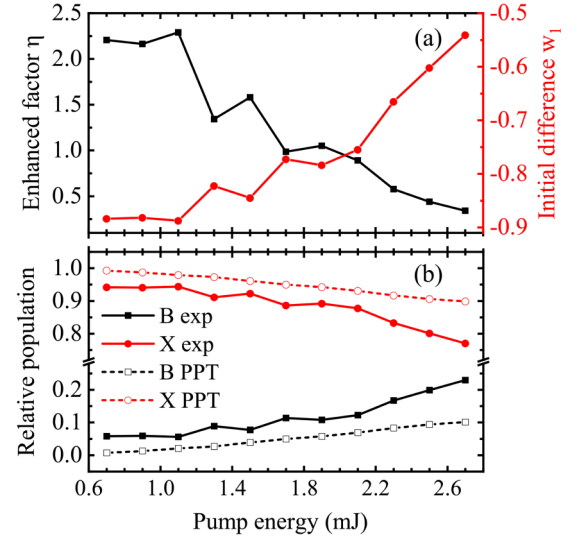


FIG. 5. (a) The enhancement factor  $\eta$  (black square) and initial relative population difference  $w_1$  (red circle). (b) The initial relative population distribution of  $N_2^+(B^2\Sigma_u^+, \nu' = 0)$  (black square) and  $N_2^+(X^2\Sigma_g^+, \nu = 0)$  (red circle) extracted from the luminescence measurement as a function of 800-nm laser energy. The relative population of  $N_2^+(B^2\Sigma_u^+, \nu' = 0)$  (black box) and  $N_2^+(X^2\Sigma_g^+, \nu = 0)$  (red circle) is calculated by the PPT model as a comparison.

value agrees well with the result observed in Fig. 4(a). The result of the final population difference  $w_2$  varied with  $w_1$  is shown in Fig. 4(b).  $w_2$  changes linearly with  $w_1$ , which reads  $w_2 = 0.71w_1$ . By substituting this linear relationship in Eq. (8), we get

$$\eta = \frac{-0.29w_1}{1 + w_1}. \quad (12)$$

According to Eq. (4), the enhancement factor  $\eta$  (black square) is obtained through the fluorescence intensity measurement as can be seen in Fig. 5(a). With 800-nm pump energy increasing from 0.7 to 2.7 mJ,  $\eta$  reduces from about 2.2 to 0.3. The initial relative population difference  $w_1$  is inversely solved from Eq. (12), which is negative. It rises with 800-nm pump energy as displayed in Fig. 5(a) (red circle). Then we acquire the initial relative population distribution of these two vibrational electronic states by Eqs. (6a) and (6b). Figure 5(b) shows that under low pump energy, the nitrogen molecular ions are most populated in the ground state  $N_2^+(X^2\Sigma_g^+, \nu = 0)$  (red circle). When the 800-nm laser exceeds 2.1 mJ,  $n_X^i$  decreases significantly, corresponding to a rapid increase of  $n_B^i$  (black square). With a pump energy of 2.7 mJ, there are 23% nitrogen molecular ions populated in the  $N_2^+(B^2\Sigma_u^+, \nu = 0)$  state. As a comparison to our results extracted from the luminescence measurement, the initial relative population of  $N_2^+(X^2\Sigma_g^+, \nu = 0)$  and  $N_2^+(B^2\Sigma_u^+, \nu' = 0)$  with ionization potentials being 15.581 and 18.875 eV, respectively, are calculated by Perelemov, Popov, and Trentev's model (PPT model) under the tunnel limit [33–35]. The laser peak intensity, which is a quite important parameter for the PPT ionization model, is hard to perform a direct measurement. Numerical simulations have been intensively employed to investigate the laser intensity during propagation of a fem-

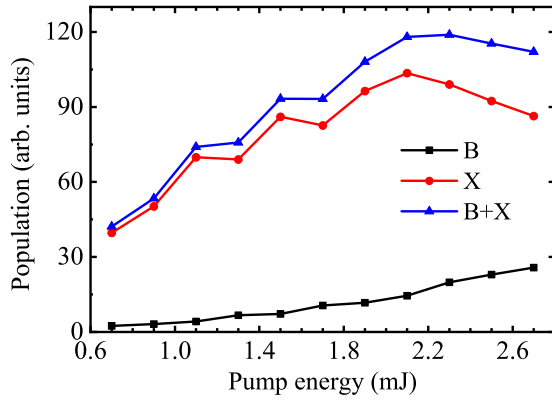


FIG. 6. The initial populations of  $N_2^+(B^2\Sigma_u^+, \nu' = 0)$  (black square),  $N_2^+(X^2\Sigma_g^+, \nu = 0)$  (red circle), and the sum (blue triangle) at a fluorescence level as a function of 800-nm pump energy.

to-second pulse in air, where an intensity ranging from a few  $10^{13}$  to  $10^{15}$  W/cm<sup>2</sup> has been reported, strongly dependent on the external focusing geometry [1,36,37]. A recent study showed that the laser intensity increased linearly with the incident laser energy until  $1.45 \times 10^{14}$  W/cm<sup>2</sup>, corresponding to a laser energy of 2 mJ with a focus lens of 1000 mm in air. Upon an increase of incident laser power, the filament peak intensity was clamped [38]. By using a much shorter lens ( $f = 150$  mm), the clamped intensity is believed to be achieved beyond the laser energy of 2.7 mJ, which is the maximal incident energy in our experiment. The laser intensity is calculated to be  $F = \frac{E_p}{\tau_e s}$ , where  $E_p$ ,  $\tau_e$ , and  $s$  are the 800-nm laser energy, the laser pulse duration of 85 fs, and the focal spot size. The accurate focal spot was measured by a CCD camera with a pixel size of  $3.2 \mu\text{m} \times 3.2 \mu\text{m}$ . Using *Matlab* to read the actual focal spot, the size is  $11 \ 141.12 \mu\text{m}^2$  (1088 pixels), which corresponds to a circle size with a radius of  $60 \mu\text{m}$ . As illustrated in Fig. 5(b),  $n_B^i$  obtained from the luminescence measurement (black square) is larger than that from the PPT model calculation (black box). This phenomenon is mainly caused by the choice of start time in our simulation, which could change the slope in Fig. 4(b). Regardless of the difference of values, for a pump energy below 2.1 mJ they share a growth rate—a key in strong-field ionization. With an 800-nm pulse energy more than 2.1 mJ,  $n_B^i$  from the luminescence measurement rises faster than that

from the PPT model calculation, implying that another effect occurs.

To gain further insight,  $N_B^i (I_{800}^{391} + I_{800}^{428})$  and  $N_X^i$  calculated by the relative population distribution are shown in Fig. 6. It can be seen that most ions are populated in  $N_2^+(X^2\Sigma_g^+, \nu = 0)$  for this two-level system. There is an unexpected drop of  $N_X^i$  after the pump energy exceeds 2.1 mJ. The sum of  $N_X^i$  and  $N_B^i$  [Fig. 6 (blue triangle)] also decreases from 2.1 to 2.7 mJ. This result supports the theoretical model of storage of population in the intermediate state  $N_2^+(A^2\Pi_u)$  with an ionization potential of 16.699 eV [5,39]. Briefly, the falling edge of the 800-nm pump laser could not ionize nitrogen but is still strong enough, inducing a strong coupling between  $N_2^+(X^2\Sigma_g^+, \nu = 0)$  and  $N_2^+(A^2\Pi_u, \nu'' = 2)$  with a resonant wavelength of 787 nm [5,40]. Population transfers efficiently from  $N_2^+(X^2\Sigma_g^+, \nu = 0)$  to  $N_2^+(A^2\Pi_u, \nu'' = 2)$ , which may result in the drop of  $N_X^i$  as shown in Fig. 6. Nevertheless, further investigations and a more detailed study need to be undertaken to ascertain this drop.

#### IV. CONCLUSION

In conclusion, we have performed experimental and numerical investigations on the populations of nitrogen molecular ions in strong laser fields. Strong couplings between the ground  $N_2^+(X^2\Sigma_g^+, \nu = 0)$  and the excited  $N_2^+(B^2\Sigma_u^+, \nu' = 0)$  state under the near-resonant laser field are demonstrated by solving the optical Bloch equations. The efficient population transfer from the ground to the excited state induced by a 400-nm pulse leads to a fluorescence enhancement of 391 and 428 nm. The population information of the ground state and excited state is simultaneously obtained based on the fluorescence enhancement factor. We believe our studies have important implications for investigating the ground- and excited-state dynamics of molecular ions in intense laser fields.

#### ACKNOWLEDGMENTS

This work was supported by the National Natural Science Foundation of China (Grants No. U1932133, No. 11905089, and No. 22075117), the Natural Science Foundation of Gansu Province, China (Grant No. 20JR5RA222), and the Fundamental Research Funds for the Central Universities (Grant No. lzujbky-2020-14).

[1] A. Couairon and A. Mysyrowicz, *Phys. Rep.* **441**, 47 (2007).  
 [2] S. L. Chin, S. Hosseini, W. Liu, Q. Luo, F. Théberge, N. Aközbe, A. Becker, V. Kandidov, O. Kosareva, and H. Schröder, *Can. J. Phys.* **83**, 863 (2005).  
 [3] A. Becker, N. Aközbe, K. Vijayalakshmi, E. Oral, C. Bowden, and S. L. Chin, *Appl. Phys. B* **73**, 287 (2001).  
 [4] S. Mitryukovskiy, Y. Liu, P. Ding, A. Houard, A. Couairon, and A. Mysyrowicz, *Phys. Rev. Lett.* **114**, 063003 (2015).  
 [5] J. Yao, S. Jiang, W. Chu, B. Zeng, C. Wu, R. Lu, Z. Li, H. Xie, G. Li, C. Yu, Z. Wang, H. Jiang, Q. Gong, and Y. Cheng, *Phys. Rev. Lett.* **116**, 143007 (2016).

[6] L. V. Keldysh, *Zh. Eksp. Teor. Fiz.* **47**, 1945 (1964) [*Sov. Phys. JETP* **20**, 1307 (1965)].  
 [7] J. Muth-Böhm, A. Becker, and F. H. M. Faisal, *Phys. Rev. Lett.* **85**, 2280 (2000).  
 [8] X.-M. Tong, Z. X. Zhao, and C.-D. Lin, *Phys. Rev. A* **66**, 033402 (2002).  
 [9] D. Pavičić, K. F. Lee, D. M. Rayner, P. B. Corkum, and D. M. Villeneuve, *Phys. Rev. Lett.* **98**, 243001 (2007).  
 [10] B. K. McFarland, J. P. Farrell, P. H. Bucksbaum, and M. Gühr, *Science* **322**, 1232 (2008).

- [11] O. Smirnova, Y. Mairesse, S. Patchkovskii, N. Dudovich, D. Villeneuve, P. Corkum, and M. Y. Ivanov, *Nature (London)* **460**, 972 (2009).
- [12] A. Becker, A. Bandrauk, and S. L. Chin, *Chem. Phys. Lett.* **343**, 345 (2001).
- [13] A. Talebpour, S. Petit, and S. L. Chin, *Opt. Commun.* **171**, 285 (1999).
- [14] E. Arévalo and A. Becker, *Phys. Rev. A* **72**, 043807 (2005).
- [15] M. V. Ammosov, N. B. Delone, and V. P. Krařnov, *Zh. Eksp. Teor. Fiz.* **91**, 2008 (1986) [*Sov. Phys. JETP* **64**, 1191 (1986)].
- [16] A. Talebpour, C. Y. Chien, and S. L. Chin, *J. Phys. B* **29**, L677 (1996).
- [17] D.-S. Guo, R. R. Freeman, and Y.-S. Wu, *Phys. Rev. A* **58**, 521 (1998).
- [18] M. J. DeWitt, E. Wells, and R. R. Jones, *Phys. Rev. Lett.* **87**, 153001 (2001).
- [19] J. Yao, G. Li, C. Jing, B. Zeng, W. Chu, J. Ni, H. Zhang, H. Xie, C. Zhang, H. Li, H. Xu, S. L. Chin, Y. Cheng, and Z. Xu, *New J. Phys.* **15**, 023046 (2013).
- [20] Y. Liu, P. Ding, N. Ibrakovic, S. Bengtsson, S. Chen, R. Danylo, E. R. Simpson, E. W. Larsen, X. Zhang, Z. Fan, A. Houard, J. Mauritsson, A. L'Huillier, C. L. Arnold, S. Zhuang, V. Tikhonchuk, and A. Mysyrowicz, *Phys. Rev. Lett.* **119**, 203205 (2017).
- [21] H. Li, M. Hou, H. Zang, Y. Fu, E. Lötstedt, T. Ando, A. Iwasaki, K. Yamanouchi, and H. Xu, *Phys. Rev. Lett.* **122**, 013202 (2019).
- [22] J. Chen, J. Yao, H. Zhang, Z. Liu, B. Xu, W. Chu, L. Qiao, Z. Wang, J. Fatome, O. Faucher, C. Wu, and Y. Cheng, *Phys. Rev. A* **100**, 031402(R) (2019).
- [23] Q. Wang, R. Chen, J. Zhao, C. Sun, X. Wang, J. Ding, Z. Liu, and B. Hu, *Chin. Phys. B* **29**, 013301 (2020).
- [24] R. Danylo, X. Zhang, Z. Fan, D. Zhou, Q. Lu, B. Zhou, Q. Liang, S. Zhuang, A. Houard, A. Mysyrowicz, E. Oliva, and Y. Liu, *Phys. Rev. Lett.* **123**, 243203 (2019).
- [25] J. Ni, W. Chu, C. Jing, H. Zhang, B. Zeng, J. Yao, G. Li, H. Xie, C. Zhang, H. Xu, S. L. Chin, Y. Cheng, and Z. Xu, *Opt. Express* **21**, 8746 (2013).
- [26] M. Lei, C. Wu, Q. Liang, A. Zhang, Y. Li, Q. Cheng, S. Wang, H. Yang, Q. Gong, and H. Jiang, *J. Phys. B: At., Mol. Opt. Phys.* **50**, 145101 (2017).
- [27] S. A. Wade, S. F. Collins, and G. W. Baxter, *J. Appl. Phys.* **94**, 4743 (2003).
- [28] C. Santori, P. Tamarat, P. Neumann, J. Wrachtrup, D. Fattal, R. G. Beausoleil, J. Rabeau, P. Olivero, A. D. Greentree, S. Praver, F. Jelezko, and P. Hemmer, *Phys. Rev. Lett.* **97**, 247401 (2006).
- [29] L. Allen and J. H. Eberly, *Optical Resonance and Two-Level Atoms* (Dover, New York, 1987).
- [30] C. Cohen-Tannoudji, J. Dupont-Roc, and G. Grynberg, *Atom-Photon Interactions: Basic Processes and Applications* (Wiley, New York, 1998).
- [31] S. Pancheshnyi, S. Starikovskaia, and A. Y. Starikovskii, *J. Phys. D* **32**, 2219 (1999).
- [32] S. R. Langhoff and C. W. Bauschlicher, Jr., *J. Chem. Phys.* **88**, 329 (1988).
- [33] F. Ilkov, J. Decker, and S. L. Chin, *J. Phys. B* **25**, 4005 (1992).
- [34] A. Talebpour, S. Larochelle, and S. L. Chin, *J. Phys. B* **31**, L49 (1998).
- [35] A. Talebpour, J. Yang, and S. L. Chin, *Opt. Commun.* **163**, 29 (1999).
- [36] P. P. Kiran, S. Bagchi, C. L. Arnold, S. R. Krishnan, G. R. Kumar, and A. Couairon, *Opt. Express* **18**, 21504 (2010).
- [37] P. P. Kiran, S. Bagchi, S. R. Krishnan, C. L. Arnold, G. R. Kumar, and A. Couairon, *Phys. Rev. A* **82**, 013805 (2010).
- [38] S. I. Mitryukovskiy, Y. Liu, A. Houard, and A. Mysyrowicz, *J. Phys. B: At., Mol. Opt. Phys.* **48**, 094003 (2015).
- [39] H. Xu, E. Lötstedt, A. Iwasaki, and K. Yamanouchi, *Nat. Commun.* **6**, 8347 (2015).
- [40] A. Lofthus and P. H. Krupenie, *J. Phys. Chem. Ref. Data* **6**, 113 (1977).